

Predictive FEM modeling of dry sliding wear in WC-Co incorporating UMESHMOTION and sliding-distance scaling

Kaweewat Worasaen^{a*}

^aDepartment of Information and Production Technology Management (IPTM), College of Industrial Technology (CIT), King Mongkut's University of Technology North Bangkok, 1518 Pracharaj 1, 10800, Bangkok, Thailand

ARTICLE INFO

Article history:

Received 22 December 2025

Accepted 3 March 2026

Available online

4 March 2026

Keywords:

Dry sliding wear

Finite element method

UMESHMOTION

Tungsten carbide

Pin-on-disk

Archard's law

ABSTRACT

This study presents a finite element modeling framework for predicting dry sliding wear in WC-Co by integrating Archard's wear law with the UMESHMOTION subroutine in Abaqus. Pin-on-disk experiments were conducted to obtain the steady-state friction coefficient, wear coefficient, and surface profile, which were used to calibrate the numerical model. A short sliding distance of 1 mm was simulated and subsequently scaled to represent a 1000 m sliding test, enabling substantial reduction in computational cost. The model accurately reproduced the experimental wear behavior, predicting a maximum wear depth within 8% relative error (0.23 μm simulated vs. 0.25 μm measured), and captured the overall geometry of the wear track. Sensitivity analysis confirmed the linear dependence of wear depth on the wear coefficient and sliding distance, supporting the validity of the scaling strategy. The results demonstrate that combining FEM, UMESHMOTION, and a sliding-distance scaling approach provides an efficient and reliable method for long-distance wear prediction in hard materials. This framework is applicable to tribological component design and can be extended to more complex multi-physics wear mechanisms in future studies.

© 2026 Growing Science Ltd. All rights reserved.

1. Introduction

Wear is the gradual damage to materials that occur at the interface of two surfaces in relative motion. This phenomenon is particularly significant in mechanical systems operating under dry sliding conditions, where the absence of lubrication intensifies frictional interactions and accelerates surface degradation. Tungsten carbide-cobalt (WC-Co) is widely recognized for its exceptional hardness and wear resistance, making it suitable for cutting tools, dies, and high-load components (Prakash, 1995; Tulhoff, 2000; Pirso et al., 2004; Iakovakis et al., 2021). Nevertheless, WC-Co components still experience progressive damage over time, especially under high contact loads and repetitive sliding conditions (Katiyar et al., 2016).

The pin-on-disk test is one of the most widely accepted laboratory techniques for investigating tribological behavior under controlled conditions. Key parameters such as friction force, wear depth, and surface morphology can be systematically measured using this method (Khuengpukheiw et al., 2021; Zamri et al., 2024; ASTM G99-17). Although experimental data are essential for understanding wear behavior, the high cost and long testing duration represent significant limitations. Moreover, experimental techniques provide limited access to subsurface stress and strain fields that govern wear mechanisms, further constraining comprehensive analysis.

In parallel with experimental approaches, the finite element method (FEM) has emerged as a powerful and versatile tool for simulating contact, friction, and material removal during sliding. Early FEM-based wear models were developed using continuum mechanics frameworks combined with Archard's wear law (Archard, 1953) to predict wear depth and surface evolution (Pödra & Andersson, 1999; Berthier et al., 1988). Since then, FEM-based wear modeling has been extensively developed and applied to a wide range of tribological systems (Daves et al., 2016; Mary & Fouvry, 2007; Curreli et al., 2018).

The incorporation of user-defined subroutines, such as UMESHMOTION in Abaqus, enables dynamic mesh updating to explicitly simulate material removal during wear processes. This capability has been successfully applied in three-dimensional pin-on-disk wear simulations (Bastola et al., 2022), showing good agreement between numerical predictions and experimental

* Corresponding author.

E-mail addresses: kaweewat.w@cit.kmutnb.ac.th (K. Worasaen)

observations (Bortoleto et al., 2013; Schmidt et al., 2018). Further developments have introduced thermal effects and advanced friction formulations into FEM-based wear models to improve predictive accuracy (Gan et al., 2021). In addition to mechanical wear, chemical and electrochemical effects can also contribute to material degradation; however, these mechanisms have received comparatively limited attention in the literature (Liu et al., 2022). To address this gap, coupled mechanical–chemical wear models have been proposed to investigate fretting corrosion phenomena (Fallahnezhad et al., 2018).

Despite these advances, most FEM-based wear simulations have focused on ductile or relatively soft materials, such as steels, aluminum alloys, and polymers (Lim, 1998; Bose & Ramkumar, 2019; Joshi & Ramkumar, 2022). In contrast, numerical modeling of wear in hard and brittle materials such as WC–Co remains relatively scarce. Some studies have examined the wear behavior of cemented carbides using FEM approaches without incorporating dynamic mesh updating to capture progressive material removal (Lim, 1998). Experimental investigations of WC–Co under dry sliding against steel or ceramic counterbodies are available (Wang et al., 2019; Attanasio et al., 2010; Attanasio et al., 2017), yet comprehensive simulation-based validation studies remain limited.

Another major challenge in wear simulation is the representation of long-duration sliding processes. Practical wear tests often involve sliding distances in the order of hundreds or thousands of meters, which are computationally prohibitive to simulate directly. To overcome this limitation, extrapolation and scaling techniques have been widely adopted, in which wear predictions obtained from short sliding distances are scaled to represent long-term behavior (Tandler et al., 2020; Imran et al., 2023; Shu et al., 2023). The reliability of such approaches depends critically on accurate calibration of wear coefficients and validation against experimental measurements.

The present study addresses these challenges by developing a three-dimensional FEM framework to predict dry sliding wear in WC–Co under pin-on-disk conditions. The model employs a user-defined UMESHMOTION subroutine implementing Archard’s wear law and incorporates experimentally calibrated values of the wear coefficient and friction coefficient. A short sliding distance of 1 mm is simulated and subsequently scaled to represent a total sliding distance of 1000 m observed in experiments. Predicted wear depth and wear scar profiles are compared with experimental measurements to validate the model. The results provide insight into the applicability and limitations of FEM-based wear simulation for hard materials and outline directions for future improvements in predictive tribological modeling.

2. Materials and Methods

2.1 Materials

WC–Co specimens were employed as the deformable disk material. Their elastic–plastic properties and Johnson–Cook constitutive parameters are summarized in Tables 1 and 2, respectively (Rashed et al., 2016). A silicon nitride (Si_3N_4) ball with a diameter of 6 mm was used as the rigid counterface.

Table 1. Mechanical properties of tungsten carbide with a cobalt binder.

Materials Name	Specific gravity (g/cc)	Young's modulus (GPa)	Poissons ratio
Tungsten carbide	14.90	630	0.21

Table 2. Johnson–Cook plasticity parameters of tungsten carbide with a cobalt binder.

Materials Name	A (MPa)	B (MPa)	n	C	m	Melting point (K)
Tungsten carbide	1506	177	0.12	0.016	0.21	1723

2.2 Pin-on-disk test

Dry pin-on-disk wear tests were conducted following the ASTM G99-05 standard, (ASTM G99-17, 2017) which defines the procedures for specimen preparation, testing configuration, and wear measurement. The Anton Paar Tribometer TRB3 model was used to perform the test in this research. Tungsten carbide (WC–Co) disks were prepared with a diameter of 20 mm and a thickness of 5 mm. A silicon nitride (Si_3N_4) ball with a diameter of 6 mm was used as the counterface material.

All specimens were ultrasonically cleaned in acetone for 10 minutes before and after each test to eliminate surface contaminants, then dried using hot and cold air in sequence. The tests were carried out under a constant normal load of 5 N at ambient temperature (approximately 25 °C). A rotational speed of 500 rpm and a wear track radius of 5 mm were applied, yielding a total sliding distance of 1000 meters.

The evolution of the coefficient of friction (μ) was continuously recorded during the test using built-in force sensors of the tribometer. A stable value of μ was extracted from the steady-state region and used for simulation calibration. After testing, the resulting wear track was measured using a white light confocal profilometer equipped on the Rtec MFT-5000 Multi-Function Tribometer. The measurements were performed with a Nikon CF Plan OFN25 WD4.7 objective lens at 20×

magnification, and each reported value represents the average of three independent measurements to determine the maximum wear depth and wear volume. The wear coefficient (k) was calculated using Archard's law:

$$k = \frac{V}{P \cdot s} \quad (1)$$

where V is the measured wear volume (mm^3), P is the applied load (N), and s is the total sliding distance (mm). Both the experimentally determined values of k and μ were used as input parameters in the FEM simulation model to ensure consistency between experimental and numerical frameworks. Each test was repeated three times, and the average values were used for analysis.

2.3 Numerical Methodology for Sliding Wear

The finite element simulation was carried out using Abaqus/Standard to model the dry sliding wear behavior of WC-Co under pin-on-disk conditions. A 3D model of the test setup was constructed, consisting of a rigid spherical pin (diameter 6 mm) and a cylindrical WC-Co disk (diameter 20 mm, thickness 5 mm). The disk was modeled as a de-formable body, while the pin was treated as an analytically rigid surface.

The simulation domain was discretized using C3D8R hexahedral elements with reduced integration. A refined mesh was applied in the contact region, with an element size of 0.02 mm, to accurately capture the contact pressure and local deformation. The boundary conditions included full constraints at the bottom face of the disk, while a vertical load of 5 N was applied to the pin through a reference point. The pin was then displaced horizontally by 1 mm along the Z-axis to simulate linear sliding.

Contact interactions between the pin and the disk were defined using a surface-to-surface contact formulation with penalty friction, and the coefficient of friction was set to $\mu = 0.68$, based on experimental measurements. Mesh distortion due to wear was handled using Arbitrary Lagrangian-Eulerian (ALE) adaptive meshing, activated on the top surface of the disk. The solver step was defined as Static General, suitable for quasistatic simulation with implicit integration.

2.4 Wear modelling

The dry sliding wear behavior of WC-Co under pin-on-disk conditions was simulated using a 3D finite element model in Abaqus/Standard, with material removal modeled via a user-defined subroutine (UMESHMOTION) based on Archard's wear law. At each increment, the subroutine accessed nodal contact variables including the average contact pressure (CSTRESS) and sliding displacement (CDISP). The wear depth (h) at each contact node was then computed using:

$$h = k \cdot p \cdot \Delta s \quad (2)$$

where k is the experimentally determined wear coefficient, p is the contact pressure, and Δs is the local sliding distance increment.

The resulting wear increment was applied as a nodal displacement in the $-Y$ direction, simulating progressive material loss. These nodal updates were communicated back to the solver, effectively altering the contact surface geometry and influencing the subsequent distribution of stress and contact pressure.

To ensure the stability and accuracy of the mesh throughout the simulation, Arbitrary Lagrangian-Eulerian (ALE) adaptive meshing was activated on the worn surface. ALE decouples mesh motion from material deformation, enabling the mesh to adapt and re-distribute nodes in regions of high distortion. This is essential in wear-simulations, where continuous nodal shifting can lead to severe element distortion if not properly managed.

In the implementation, mesh smoothing was enabled through the LSMOOTH flag within the subroutine (LSMOOTH = 1), which instructs Abaqus to apply internal smoothing algorithms after each mesh update. This reduces sharp gradients in element distortion and preserves element aspect ratio, particularly near the wear front. Additionally, node motion was confined to the normal direction only, minimizing tangential distortion. Stability was monitored through convergence behavior and element Jacobian values; no critical mesh errors were observed during the full simulation cycle.

Due to the computational cost of simulating long sliding distances (e.g., 1000 m), only a 1 mm sliding motion was modeled directly. A scaling strategy was then applied, assuming linear proportionality between wear depth and sliding distance as per Archard's law. The resulting wear profile was linearly extrapolated to represent long-term behavior and was compared against experimental profilometer data.

The combination of UMESHMOTION and ALE mesh smoothing thus provided a robust framework for simulating progressive wear with stable mesh quality, accurate contact mechanics, and realistic scar evolution over extended sliding distances.

2.5 Wear simulation procedure

The wear simulation was implemented as a repetitive and incremental computational process, wherein material removal due to sliding contact was accumulated over time. At each increment, the simulation proceeded through a sequence of four key steps. First, the nonlinear contact problem was solved using finite element analysis to obtain the distribution of contact pressure across the interface between the Si_3N_4 ball and WC-Co disk. This pressure distribution served as a critical input for the subsequent wear calculation. Next, the wear depth at each contact node was computed using Archard's wear law, which relates the local contact pressure and sliding distance to the volumetric wear loss via the wear coefficient (k), previously obtained from experimental tests. This step provided a quantification of the material loss at the current increment. Due to the high computational cost associated with directly simulating long sliding distances (e.g., 1000 m), a scaling strategy was employed. Specifically, the results from a short-range simulation with 1 mm of sliding were linearly extrapolated, under the assumption that wear depth is directly proportional to sliding distance. This approach allowed for an efficient yet representative prediction of long-term wear behavior while keeping the computational time within practical limits. Finally, the computed wear depth was applied to the contact nodes through the combined use of the UMESHMOTION subroutine and the Arbitrary Lagrangian-Eulerian (ALE) adaptive meshing technique. This step dynamically updated the geometry of the contact surface while preserving mesh quality and simulation stability throughout the deformation process. This iterative process, encompassing contact resolution, wear computation, and mesh adaptation, continued until the prescribed sliding displacement was represented. The methodological workflow is depicted in **Fig. 1**.

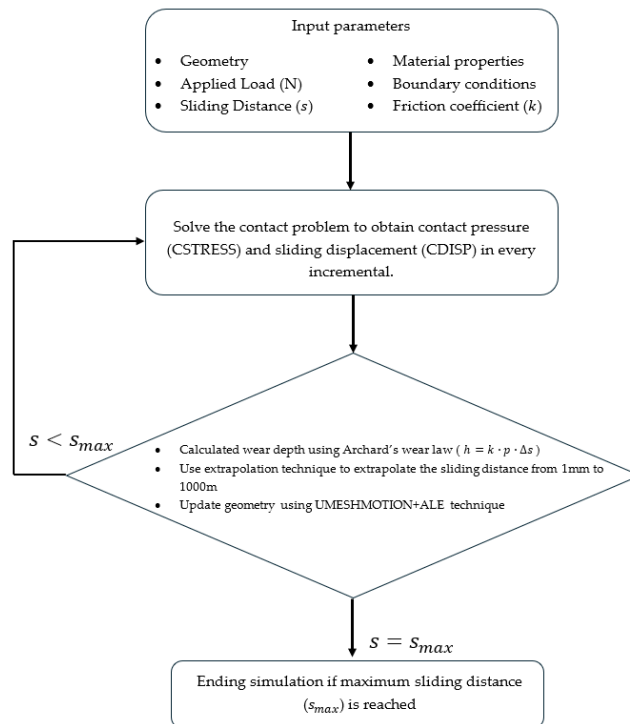


Fig. 1. Flowchart illustrates the numerical wear simulation procedure using the finite element method (FEM) and UMESHMOTION subroutine.

2.5.1 Numerical model

To simulate the dry sliding wear behavior of tungsten carbide (WC-Co), both two-dimensional and three-dimensional finite element (FE) models of the pin-on-disk tribometer were developed using ABAQUS/Standard. The purpose of the 2D model was to perform preliminary investigations with reduced computational demand, while the 3D model was later constructed to replicate the full-scale experimental configuration. In the 2D plane strain model, only a segment of the disk was represented to reduce computational cost. The geometry matched the experimental specimen, as illustrated in **Fig. 2**, and the domain was discretized using four-node quadrilateral plane strain elements (CPE4). The WC-Co disk was modeled as a linearly elastic deformable body, with material properties summarized in Table 1 and 2 respectively, while the Si_3N_4 pin was treated as a rigid body to simplify the simulation and reflect the negligible deformation observed during experiments. A very fine mesh was applied at the contact interface, with a minimum element size of 0.02 mm, determined through a mesh convergence study to ensure solution accuracy. A vertical load of 5 N was applied to the pin, and a horizontal displacement was used to simulate

sliding motion. Thermal effects were neglected under the assumption that frictional heating was insufficient to alter material properties. Since experimental observations indicated negligible wear on the pin, only the disk surface was considered in the wear simulation. The contact problem in both 2D and 3D models was formulated using a surface-to-surface contact algorithm with the master–slave approach, where the pin acted as the master surface and the disk as the slave. Tangential behavior was defined by Coulomb’s friction law, with the coefficient of friction obtained from experimental tests. Contact enforcement was performed using the penalty method, allowing for controlled inter-facial behavior and efficient convergence.

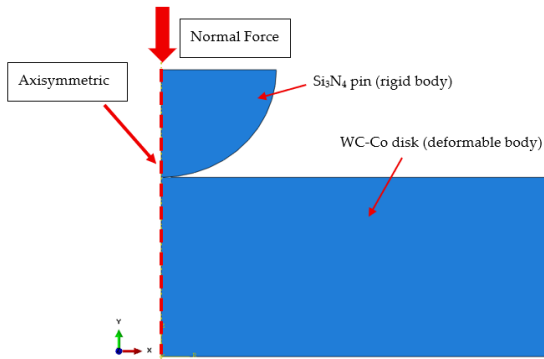


Fig. 2. The 2D Finite element model configuration for the axisymmetric simulation of the pin-on-disk test. The model consists of a Si₃N₄ pin, modeled as a rigid body, in contact with a WC-Co disk, modeled as a deformable body.

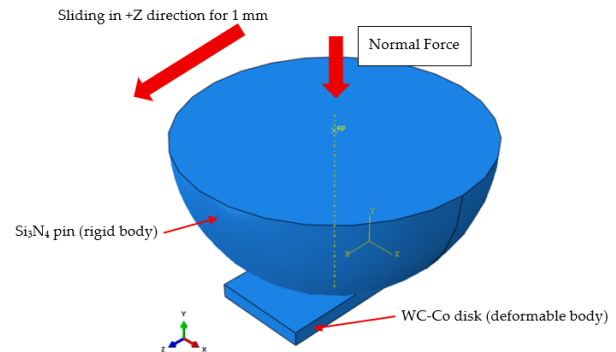


Fig. 3. Schematic representation of the 3D finite element model for the pin-on-disk wear simulation.

To model wear progression, the UMESHMOTION user subroutine was employed in conjunction with the Arbitrary Lagrangian-Eulerian (ALE) adaptive meshing technique. Contact pressure (CSTRESS) and sliding displacement (CDISP) were extracted at each increment and passed into UMESHMOTION, which calculated the nodal displacement due to wear based on Archard’s law. This displacement was used to update the geometry, while ALE smoothing preserved element quality during mesh deformation. Following the initial calibration in 2D, a full 3D model of the pin-on-disk setup was constructed, as illustrated in **Fig. 3**, using the same experimental dimensions. The 3D model provided a more realistic representation of the wear track and contact pressure distribution, enabling direct comparison with the profilometer measurements obtained from the wear experiments.

2.5.2 Mesh convergence analysis

To ensure the accuracy of contact pressure prediction in the wear simulation, a mesh convergence study was conducted using the 2D plane strain model. The objective was to identify an optimal element size in the contact region that would allow the finite element solution to closely approximate the analytical Hertzian contact pressure distribution (Ahmadi & Sadeghi, 2022) under a normal load of 5 N. A series of simulations were performed with mesh sizes ranging from 0.05 mm to 0.01 mm. As the mesh was refined, the FEM results showed improved agreement with the Hertz solution. Specifically, reducing the mesh size from 0.05 mm to 0.01 mm resulted in a noticeable convergence toward the analytical profile. A subsequent evaluation using a 0.02 mm mesh demonstrated a deviation of less than 5% compared to the 0.01 mm case, indicating negligible loss of accuracy.

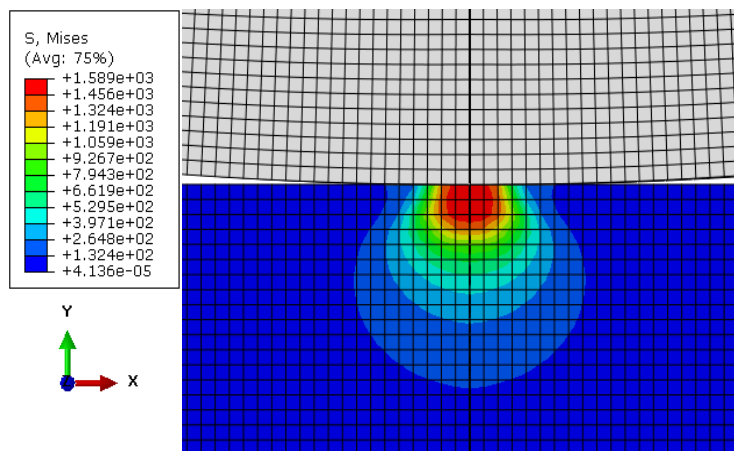


Fig. 4. Comparison between the finite element–predicted contact pressure distribution and the analytical Hertzian solution for the finest mesh size (0.01 mm) used in the mesh convergence study. The close agreement between the simulated and analytical

curves confirms that the selected mesh resolution accurately captures the localized contact mechanics under a 5 N normal load. Therefore, a mesh size of 0.02 mm was selected as the optimal resolution for the contact interface, providing a balance between computational efficiency and solution fidelity. The results of this convergence study are presented in **Fig. 4**. In addition to contact pressure convergence, a mesh sensitivity analysis was also conducted with respect to the von Mises stress in the contact zone. As shown in **Fig. 5**, the peak von Mises stress values varied significantly with coarser meshes but stabilized once the mesh size was reduced to 0.02 mm or smaller. This further confirms that 0.02 mm is a suitable mesh size for resolving stress fields in the critical contact region while avoiding excessive computational cost.

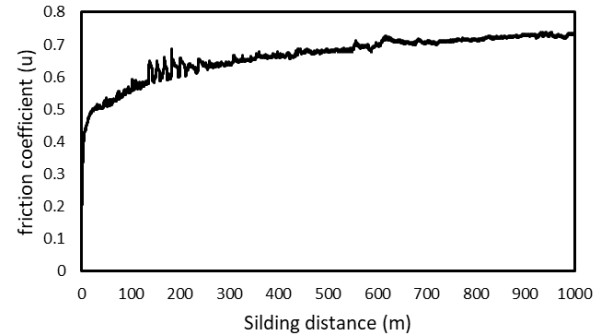
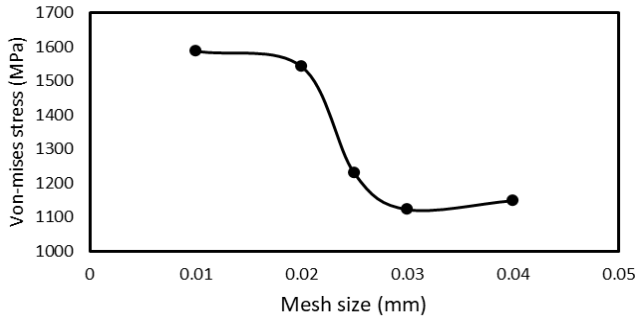


Fig. 5. Effect of mesh refinement on the peak von Mises stress in the contact region. Coarser meshes (0.05–0.03 mm) exhibit noticeable deviations in stress magnitude, while meshes of 0.02 mm and finer show convergent behavior. This result supports the selection of a 0.02 mm element size as an optimal balance between computational efficiency and accuracy.

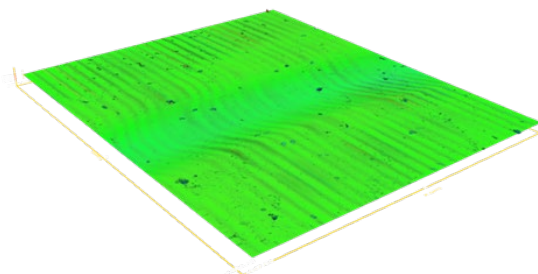
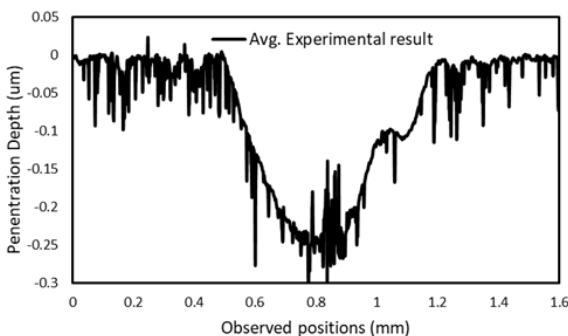
Fig. 6. Variation of the friction coefficient (μ) with sliding distance during the dry sliding wear test of WC-Co against the counterface material.

3. Results and Discussions

This section presents the comparison between experimental and numerical results, evaluates the model performance, and discusses the factors influencing the accuracy of FEM-based wear prediction.

3.1 Experimental Results

The tribological experiment using a pin-on-disk tribometer under dry sliding conditions produced valuable data for validating the numerical model. The measured friction coefficient throughout the test stabilized around 0.68, indicating a relatively consistent contact behavior between the WC-Co disk and Si₃N₄ ball. As shown in Figure 6, the coefficient of friction exhibited an initial transient phase, followed by a gradual stabilization. The early-stage fluctuations, particularly in the first 200 meters, are attributed to the running-in process and asperity interactions. After approximately 300 meters, the curve plateaued, suggesting that steady-state sliding was achieved. This behavior is typical of ceramic–metal tribopairs under unlubricated conditions, where micro-wear and surface adaptation dominate the early stage.



(a)

(b)

Fig. 7. a) Experimental wear depth profiles averaged from five equally spaced cross-sections across the wear scar. b) 3D surface topography of the WC-Co disk after dry sliding wear, captured using optical profilometry.

The 3D surface topography of the WC-Co disk after dry sliding wear, captured using optical profilometry and the experimental wear depth profiles averaged from five equally spaced cross-sections across the wear scar are illustrated in **Fig.**

7 (Left) and (Right), respectively. The wear track is characterized by a smooth and continuous groove along the sliding path with periodic surface ridges oriented in the sliding direction. The averaged wear depth is approximately $0.25\ \mu\text{m}$ and occurs at the center of the contact path. The symmetry and consistency of the wear profiles suggest stable tribological conditions throughout the test.

3.2 Simulation Results

The finite element simulation was conducted using a 3D pin-on-disk configuration, incorporating an ALE-based mesh updating strategy driven by the UMESHMOTION subroutine and Archard's wear law. The goal was to replicate the observed wear behavior of WC-Co under dry sliding against a Si_3N_4 ball. Given the computational limitations, a 1 mm sliding distance was used in the simulation and scaled to represent the 1000 m sliding distance in the experiment. The simulation was performed with calibrated input parameters including a friction coefficient of 0.68 and an optimized wear coefficient, as fitted from experimental data.

3.2.1 Comparison between experimental results and simulation results

The comparison between the experimental measurement and the finite element simulation for the wear profile of WC-Co under dry sliding conditions is shown in Figure 8. The experimental data (black line) exhibits a maximum penetration depth of approximately $0.25\ \mu\text{m}$ at the center of the wear track, whereas the simulation (red line) predicts a slightly shallower profile, with a maximum depth of around $0.23\ \mu\text{m}$. The overall shape of the simulated profile closely follows the experimental trend, indicating that the FEM model successfully captures the wear scar geometry and its gradual depth variation along the sliding path.

The difference in maximum depth corresponds to a relative error of about 8%, which is within an acceptable range for predictive wear modeling using Archard's law in combination with the UMESHMOTION subroutine. This deviation may result from uncertainties in the wear coefficient (k), simplifications in contact geometry, and the omission of microstructural effects such as grain pull-out or binder phase deformation, which are not explicitly modeled in the continuum approach.

Another observation is that the simulated profile exhibits a smoother curve compared to the experimental data, which shows higher surface roughness and local fluctuations. This is because the finite element model assumes an idealized contact interface with perfectly smooth initial surfaces, while the WC-Co specimen inherently contains surface asperities and microstructural heterogeneities from the manufacturing process (e.g., carbide grain protrusions, binder phase depressions) that cause local variations in wear depth. During profilometry scanning, these asperities generate small peaks and valleys along the track, leading to the high-frequency fluctuations seen in the experimental curve. These fluctuations arise from both actual surface topography variations and measurement noise from profilometry, whereas the simulation assumes a smooth surface and uniform material properties. Experimental roughness can be amplified by heterogeneous material removal mechanisms such as grain pull-out, localized micro-chipping, and preferential binder wear. Additionally, profilometer measurements are sensitive to probe tip radius, alignment, and vibration, introducing further noise into the recorded profile. In contrast, the simulation uses deterministic geometry and homogeneous mechanical properties, capturing only the average wear response predicted by Archard's law, without stochastic variation. This difference in data acquisition statistical, noisy real-world measurement versus idealized numerical computation is the main reason for the smoother simulated curve.

Despite the minor depth discrepancy, the model demonstrates strong predictive capability in both wear scar width and general depth distribution. This confirms that the calibrated wear coefficient effectively replicates real wear behavior under the tested conditions and that the linear scaling of wear depth with sliding distance remains valid.

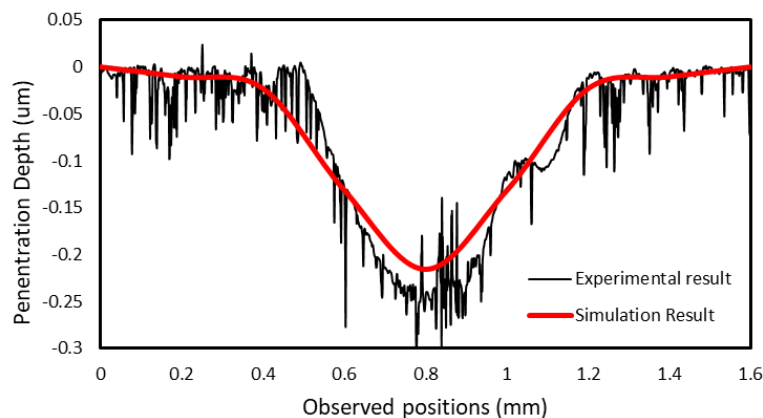


Fig. 8. Comparison of wear track profiles between experimental measurement (black line) and finite element simulation (red line) for WC-Co under dry sliding conditions.

3.2.2 Sensitivity to Sliding Distance and Wear Coefficient

A sensitivity analysis was conducted to evaluate the influence of the wear coefficient (k) on the predicted wear depth. Multiple simulations were executed by varying k within a reasonable range based on experimental calibration. As shown in **Fig. 9**, the predicted wear depth exhibited a linear relationship with respect to the wear coefficient. For instance, a k value of $5.2 \times 10^{-1} \text{ mm}^2/\text{N}$ produced a wear depth that closely matched the experimental benchmark of approximately $0.25 \mu\text{m}$. Deviations in k of $\pm 0.1 \times 10^{-1}$ led to noticeable under- or over-estimation of wear depth, highlighting the critical role of accurate coefficient fitting from experimental data. This result reinforces the assumption that wear depth in WC-Co under dry sliding follows a nearly linear scaling with sliding distance, consistent with Archard's law. Thus, the use of short sliding simulations combined with extrapolation is justified, provided that k is appropriately calibrated. To ensure the reliability and generalizability of the FEM-based wear model, a sensitivity analysis was conducted by systematically varying two critical input parameters including the wear coefficient (k) and the sliding distance. These parameters are essential in determining the wear volume governed by Archard's wear law as illustrated in Eq. (2).

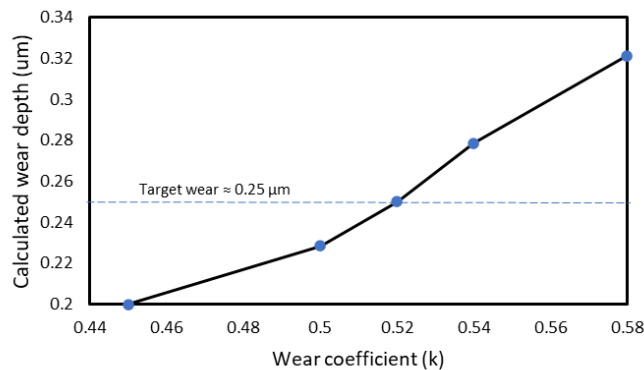


Fig. 9. Sensitivity analysis of predicted wear depth with respect to variations in the wear coefficient, using the local wear equation $\Delta h = k \cdot p \cdot \Delta s$ with constant contact pressure and a fixed sliding distance of 1 mm. The results confirm the linear influence of k on wear depth prediction.

Fig. 9 illustrates the simulated wear depth response to variations in k , while maintaining constant pressure and a fixed sliding distance of 1 mm. The results show a nearly linear relationship between k and wear depth (h), confirming the predictive behavior of Eq. (3). As k increases from 0.45 to 0.58 mm^2/N , the predicted wear depth increases from approximately $0.20 \mu\text{m}$ to $0.32 \mu\text{m}$. This trend validates the critical role of accurate wear coefficient calibration. Even slight overestimations of k can lead to significant discrepancies in wear predictions. Since p is determined by contact mechanics and Δs was fixed for scaling convenience, k becomes the dominant parameter in controlling wear depth accuracy. Furthermore, scaling the sliding distance (e.g., from 1 mm to 1000 mm) can be done proportionally in simulations due to the linear dependence of h on Δs , provided that k is experimentally validated. This makes Eq. (2) especially powerful in reducing computational time while maintaining realistic long-range wear predictions. The sensitivity to the wear coefficient was performed only for a range k values as low as 0.45 to 0.58 while all other conditions such as boundary conditions, material properties, and sliding distance were kept constant. With a preliminary evaluation of WC-Co calibration alongside the rigorous literature evaluation under the same conditions, the acceptable values of k were set as 0.45, 0.50, 0.52, 0.54, and 0.58. These values were selected based on preliminary calibration with experimental results and known literature ranges for WC-Co under similar tribological conditions. The extrapolated depths of wear for every scenario were calculated from the simulations based on the nodal displacement values in U2 (normal direction) and the maximum wear depth was documented. These measurements were used to draw results which are illustrated in **Fig. 9**. There appears to be a linear relationship between the wear coefficient and wear depth.

The figure demonstrates clearly that geometry of the wear surface developed by friction is directly sensitive to the wear coefficient (k). An increase of k values directly proportional to increase of wear depth. Assuming $k = 0.52 \text{ mm}^2/\text{N}$, the wear depth is approximately $0.25 \mu\text{m}$. This experimental value was closely matched with the model prediction. Further to this, the model prediction is sensitive to k value as shown by ± 0.03 around k value leading to as 8% under or over predicted wear depth.

Due to the computational cost associated with modeling the entire 1000 m of actual sliding, the simulation was performed for a significantly reduced sliding distance of only 1 mm. The simulation result was then scaled linearly, assuming that wear grows proportionally with sliding distance in accordance with Archard's law. This assumption is supported by experimental observations (as shown earlier in **Fig. 6**) where the friction coefficient and wear growth showed stable behavior after the running-in phase, suggesting that steady-state wear dominates. By performing the simulation over 1 mm of sliding and

applying a scaling factor of 1000, the computational time was drastically reduced while still achieving predictive accuracy. This technique allowed for iterative calibration of k within reasonable computation times, enabling efficient tuning of the model to match experimental observations.

3.2.3 Stress Analysis of the WC–Co Disk under Dry Sliding Wear

The von Mises stress distribution in the WC–Co disk after the simulated dry sliding process is shown in Figure 10. The model clearly demonstrates a localized high-stress zone at the leading edge of the wear track, corresponding to the initial contact point between the rigid indenter and the specimen surface. The maximum von Mises stress in this region reaches approximately 2.1 GPa, arising from the combined effect of normal indentation and tangential shear forces generated during sliding. These concentrated stresses play a critical role in initiating material removal, particularly in the form of micro-plastic deformation and early-stage wear particle detachment. The stress intensity decreases along the sliding path towards the trailing edge of the wear scar, creating a long, moderate stress ($\sim 1.2\text{--}1.5$ GPa) track. This spatial gradient reflects the gradual unloading of the contact zone during sliding. Areas outside the wear track are virtually stress-free (<0.2 GPa), which shows that the wear process is mechanically confined to the contact path and does not significantly affect the bulk material away from the interface. The inset in **Fig. 10** magnifies the stress field within the wear scar and reveals that the maximum stresses are concentrated just beneath the surface rather than exactly at the topmost layer. This suggests that subsurface damage such as carbide grain debonding, binder phase yielding, or micro-crack initiation is a plausible mechanism in WC–Co under repeated sliding. Additionally, narrow stress bands along the lateral edges of the track may promote micro-chipping, which aligns with observed debris formation in experimental studies of cemented carbides.

When these stress patterns are interpreted alongside the wear depth results from UMESHMOTION-based material removal, the correlation becomes clear that the regions of highest von Mises stress coincide with locations of maximum penetration depth in the wear profile (≈ 0.25 μm in experiment, ≈ 0.23 μm in simulation). The smooth distribution of simulated wear depth mirrors the deterministic stress field generated by the FEM model, while the experimental profile's fluctuations are influenced by the stochastic nature of real surface asperities and heterogeneous grain-scale failure.

This integrated interpretation confirms that the stress analysis not only identifies the mechanical origins of the wear scar geometry but also validates the predictive capability of the combined Archard's law and UMESHMOTION approach. The model's ability to replicate both the magnitude and spatial distribution of wear depth demonstrates its robustness for predictive wear modeling of WC–Co under dry sliding conditions.

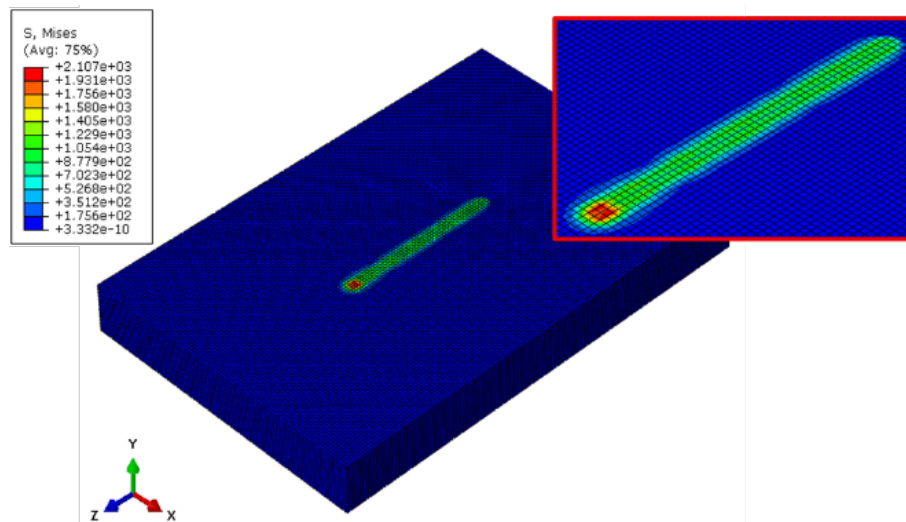


Fig. 10. Finite element simulation results showing the von Mises stress distribution in the WC–Co disk during dry sliding contact. The stress field illustrates localized high-stress concentration at the leading edge of the contact zone (red region), gradually decreasing along the sliding path (green–blue regions). The inset provides a magnified view of the contact interface, highlighting the stress gradient and mesh resolution in the wear track region.

The subsurface stress fields obtained from the FEM simulations provide additional mechanistic insight into the wear behavior of WC–Co during dry sliding. The maximum shear stress (τ_{max}) was observed to occur slightly beneath the surface, rather than at the contact interface, which is consistent with classical Hertzian contact theory and is a known precursor for micro-crack initiation and grain pull-out in hardmetal systems. This stress gradient indicates that material removal is not solely governed by surface abrasion, but also by subsurface plastic deformation and localized damage accumulation within the cobalt

binder phase. Such localized shear-driven deformation can weaken the carbide–binder interfacial strength, promoting the detachment of carbide particles and contributing to the steady-state wear mechanism observed experimentally. The FEM-predicted stress distribution therefore supports the hypothesis that mild wear in WC–Co under low-load conditions arises from a combined mechanism of surface micro-abrasion and subsurface shear-assisted material removal, aligning well with previous tribological studies on cemented carbides.

4. Conclusions

This study presented a finite element modeling approach to predict dry sliding wear in WC–Co using a scaled simulation strategy based on Archard’s wear law. By combining a short-range (1 mm) sliding simulation with a calibrated wear coefficient and leveraging the UMESHMOTION subroutine in Abaqus, the model was able to accurately reproduce the experimentally observed wear depth and profile after a 1000 m pin-on-disk test. The key findings include:

- The predicted wear depth showed excellent agreement with experimental measurements, particularly when the wear coefficient was fitted to $k = 5.2 \times 10^{-1} \text{ mm}^2/\text{N}$.
- Sensitivity analysis confirmed a nearly linear relationship between wear depth and both wear coefficient and sliding distance, validating the use of scaling in the simulation.
- The ALE (Arbitrary Lagrangian-Eulerian) adaptive meshing technique-maintained element quality and ensured stable convergence during wear progression.
- Subsurface stress analysis revealed that wear was driven by localized plastic deformation rather than brittle failure, aligning with the observed smooth wear scar morphology.

The proposed simulation method enables fast and reliable prediction of long-term wear using computationally efficient short simulations. This approach is especially useful for hard materials like WC–Co, where direct simulation of full-scale wear tests is computationally prohibitive. The methodology developed here can serve as a foundation for future work involving multi-physics wear modeling, temperature effects, and more complex contact geometries.

Although the proposed FEM–UMESHMOTION framework demonstrated strong agreement with experimental observations, several limitations should be noted. First, the model assumes perfectly smooth and homogeneous material surfaces, whereas real WC–Co contains microstructural heterogeneities such as carbide grain protrusions, binder-phase softening, and occasional micro-chipping, which are not captured in a continuum-level formulation. Second, the friction coefficient was treated as a constant value obtained from the steady-state region of the experiment; in practice, friction can vary during running-in or under evolving surface conditions. Third, thermal effects generated during dry sliding were neglected due to the relatively low load, yet temperature rise may influence material properties and wear mechanisms in high-energy conditions. Additionally, the scaling approach assumes linear wear progression according to Archard’s law; while valid for mild wear regimes, this assumption may not hold for severe wear or transition to different mechanisms.

Future work may incorporate microstructure-informed material models, coupled thermo-mechanical analysis, or position-dependent friction laws to capture more complex wear behavior. Multi-cycle simulations without linear scaling could also be explored to validate long-term predictions in higher load or higher temperature applications.

Acknowledgments

This research was funded by College of Industrial Technology, King Monkut’s University of Technology North Bangkok (Grant No. Res-CIT0309/2022)

Author Contributions

K.W.: conceptualization, investigation, reviewing and editing.

Conflicts of Interest

The authors declare no conflict of interest.

References

- Ahmadi, A., & Sadeghi, F. (2022). A three-dimensional finite element damage mechanics model to simulate fretting wear of Hertzian line and circular contacts in partial slip regime. *Journal of Tribology*, *144*, 051602. <https://doi.org/10.1115/1.4051814>
- Archard, J.F. (1953). Contact and rubbing of flat surfaces. *Journal of Applied Physics*, *24*(8), 981–988. <https://doi.org/10.1063/1.1721448>

- ASTM G99-17. (2017). *Standard test method for wear testing with a pin-on-disk apparatus*. ASTM International, West Conshohocken, PA, USA.
- Attanasio, A., Ceretti, E., Fiorentino, A., Cappellini, C., & Giardini, C. (2010). Investigation and FEM-based simulation of tool wear in turning operations with uncoated carbide tools. *Wear*, 269(5–6), 344–350. <https://doi.org/10.1016/j.wear.2010.04.013>
- Attanasio, A., Faini, F., & Outeiro, J.C. (2017). FEM simulation of tool wear in drilling. *Procedia CIRP*, 58, 440–444. <https://doi.org/10.1016/j.procir.2017.03.249>
- Bastola, A., Stewart, D., & Dini, D. (2022). Three-dimensional finite element simulation and experimental validation of sliding wear. *Wear*, 504–505, 204402. <https://doi.org/10.1016/j.wear.2022.204402>
- Berthier, Y., Vincent, L., & Godet, M. (1988). Velocity accommodation in fretting. *Wear*, 125(1–2), 25–38. [https://doi.org/10.1016/0043-1648\(88\)90191-3](https://doi.org/10.1016/0043-1648(88)90191-3)
- Bortoleto, E.M., Rovani, A.C., Seriacopi, V., Profito, F.J., Zachariadis, D.C., Machado, I.F., & Souza, R.M. (2013). Experimental and numerical analysis of dry contact in the pin-on-disc test. *Wear*, 301(1–2), 19–26. <https://doi.org/10.1016/j.wear.2012.12.005>
- Bose, K.K., & Ramkumar, P. (2019). Finite element method-based sliding wear prediction of steel-on-steel contacts using extrapolation techniques. *Proceedings of the Institution of Mechanical Engineers, Part J: Journal of Engineering Tribology*, 233, 1446–1463. <https://doi.org/10.1177/1350650119836813>
- Curreli, C., Di Puccio, F., & Mattei, L. (2018). Application of the finite element sub-modeling technique in a single point contact and wear problem. *International Journal for Numerical Methods in Engineering*, 116(5), 349–367. <https://doi.org/10.1002/nme.5940>
- Daves, W., Kubin, W., Scheriau, S., & Pletz, M. (2016). A finite element model to simulate the physical mechanisms of wear and crack initiation in wheel/rail contact. *Wear*, 366–367, 78–83. <https://doi.org/10.1016/j.wear.2016.05.027>
- Fallahnezhad, K., Oskouei, R.H., & Taylor, M. (2018). Development of a fretting corrosion model for metallic interfaces using adaptive finite element analysis. *Finite Elements in Analysis and Design*, 148, 38–47. <https://doi.org/10.1016/j.finel.2018.05.004>
- Gan, L., Xiao, K., Pu, W., Tang, T., & Wang, J.X. (2021). A numerical method to investigate the effect of thermal and plastic behaviors on the evolution of sliding wear. *Meccanica*, 56, 2339–2356. <https://doi.org/10.1007/s11012-021-01362-y>
- Iakovakis, E., Avcu, E., Roy, M.J., Gee, M., & Matthews, A. (2021). Dry sliding wear behaviour of additive manufactured CrC-rich WC–Co cemented carbides. *Wear*, 486–487, 204127. <https://doi.org/10.1016/j.wear.2021.204127>
- Imran, M., Wang, D., & Abdel Wahab, M. (2023). Three-dimensional finite element simulations of fretting wear in steel wires used in coal mine hoisting systems. *Advances in Engineering Software*, 184, 103499. <https://doi.org/10.1016/j.advengsoft.2023.103499>
- Joshi, V., & Ramkumar, P. (2022). Transient wear FEA modelling using extrapolation technique for steel-on-steel dry sliding contact. *Tribology Online*, 17, 162–174. <https://doi.org/10.2474/trol.17.162>
- Katiyar, P.K., Singh, P.K., Singh, R., & Kumar, A. (2016). Modes of failure of cemented tungsten carbide tool bits (WC/Co): A study of wear parts. *International Journal of Refractory Metals and Hard Materials*, 54, 27–38. <https://doi.org/10.1016/j.ijrmhm.2015.06.018>
- Khuengpukheiw, R., Wisitsoraat, A., & Saikaew, C. (2021). Wear behaviors of HVOF-sprayed NiSiCrFeB, WC–Co/NiSiCrFeB and WC–Co coatings evaluated using a pin-on-disc tester with C45 steel pins. *Wear*, 484–485, 203699. <https://doi.org/10.1016/j.wear.2021.203699>
- Lim, S.C. (1998). Recent developments in wear-mechanism maps. *Tribology International*, 31(1–3), 87–97. [https://doi.org/10.1016/S0301-679X\(98\)00011-5](https://doi.org/10.1016/S0301-679X(98)00011-5)
- Liu, Y., Xiang, D., Wang, K., & Yu, T. (2022). Corrosion of laser cladding high-entropy alloy coatings: A review. *Coatings*, 12, 1669. <https://doi.org/10.3390/coatings12111669>
- Mary, C., & Fouvry, S. (2007). Numerical prediction of fretting contact durability using energy wear approach: Optimisation of finite-element model. *Wear*, 263(1–6), 444–450. <https://doi.org/10.1016/j.wear.2007.01.116>
- Pirso, J., Letunovits, S., & Viljus, M. (2004). Friction and wear behaviour of cemented carbides. *Wear*, 257(3–4), 257–265. <https://doi.org/10.1016/j.wear.2003.12.014>
- Pödra, P., & Andersson, S. (1999). Simulating sliding wear with finite element method. *Tribology International*, 32(2), 71–81. [https://doi.org/10.1016/S0301-679X\(99\)00012-2](https://doi.org/10.1016/S0301-679X(99)00012-2)
- Prakash, L.J. (1995). Application of fine grained tungsten carbide based cemented carbides. *International Journal of Refractory Metals and Hard Materials*, 13, 257–264. [https://doi.org/10.1016/0263-4368\(95\)92672-7](https://doi.org/10.1016/0263-4368(95)92672-7)
- Rashed, A., Yazdani, M., Babaluo, A., & Hajizadeh Parvin, P. (2016). Investigation on high-velocity impact performance of multi-layered alumina ceramic armors with polymeric interlayers. *Journal of Composite Materials*, 50(25), 3561–3576. <https://doi.org/10.1177/0021998315622982>
- Schmidt, A.A., Schmidt, T., Grabherr, O., & Bartel, D. (2018). Transient wear simulation based on three-dimensional finite element analysis for a dry running tilted shaft-bushing bearing. *Wear*, 408–409, 171–179. <https://doi.org/10.1016/j.wear.2018.05.008>
- Shu, Y., Yang, G., & Liu, Z. (2023). Simulation research on fretting wear of train axles with interference fit based on press-fitted specimen. *Wear*, 523, 204777. <https://doi.org/10.1016/j.wear.2023.204777>

- Tandler, R., Bohn, N., Gabbert, U., & Woschke, E. (2020). Analytical wear model and its application for the wear simulation in automotive bush chain drive systems. *Wear*, 446–447, 203193. <https://doi.org/10.1016/j.wear.2020.203193>
- Tulhoff, H. (2000). Carbides: Metal-like carbides of industrial importance. In *Ullmann's Encyclopedia of Industrial Chemistry* (Electronic ed.). Wiley-VCH Verlag, Weinheim. https://doi.org/10.1002/14356007.a05_061.pub2
- Wang, Y., Su, H., Dai, J., Zhang, X., & Chen, M. (2019). A novel finite element method for the wear analysis of cemented carbide tool during high-speed cutting of Ti-6Al-4V. *International Journal of Advanced Manufacturing Technology*, 103, 2795–2807. <https://doi.org/10.1007/s00170-019-03776-1>
- Zamri, W.F.H.W., Shamsudeen, A., & Din, M.F.M. (2024). Dry sliding wear behavior of cemented carbide at elevated temperatures. *Journal of Engineering and Technological Sciences*, 56(5), 603–612. <https://doi.org/10.5614/j.eng.technol.sci.2024.56.5.5>



© 2026 by the authors; licensee Growing Science, Canada. This is an open access article distributed under the terms and conditions of the Creative Commons Attribution (CC-BY) license (<http://creativecommons.org/licenses/by/4.0/>).